

Origins of Initiation Rate Differences in Ruthenium Olefin Metathesis Catalysts Containing Chelating Benzylidenes

Keary M. Engle,[†] Gang Lu,[‡] Shao-Xiong Luo,[†] Lawrence M. Henling,[†] Michael K. Takase,[†] Peng Liu,^{*,‡,§} K. N. Houk,^{*,§} and Robert H. Grubbs^{*,†}

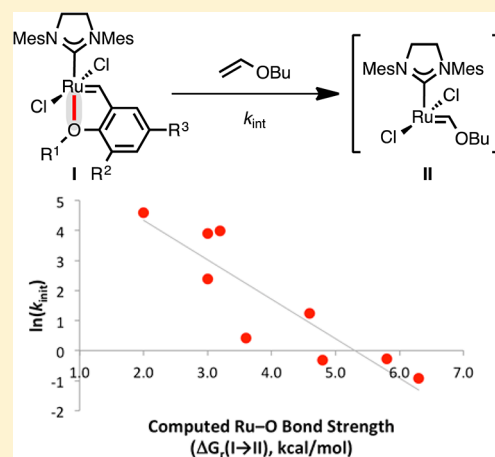
[†]Arnold and Mabel Beckman Laboratories of Chemical Synthesis, California Institute of Technology, Pasadena, California 91125, United States

[‡]Department of Chemistry, University of Pittsburgh, Pittsburgh, Pennsylvania 15260, United States

[§]Department of Chemistry and Biochemistry, University of California, Los Angeles, California 90095, United States

Supporting Information

ABSTRACT: A series of second-generation ruthenium olefin metathesis catalysts was investigated using a combination of reaction kinetics, X-ray crystallography, NMR spectroscopy, and DFT calculations in order to determine the relationship between the structure of the chelating *o*-alkoxybenzylidene and the observed initiation rate. Included in this series were previously reported catalysts containing a variety of benzylidene modifications as well as four new catalysts containing cyclopropoxy, neopentyloxy, 1-adamantyloxy, and 2-adamantyloxy groups. The initiation rates of this series of catalysts were determined using a UV/vis assay. All four new catalysts were observed to be faster-initiating than the corresponding isopropoxy control, and the 2-adamantyloxy catalyst was found to be among the fastest-initiating Hoveyda-type catalysts reported to date. Analysis of the X-ray crystal structures and computed energy-minimized structures of these catalysts revealed no correlation between the Ru–O bond length and Ru–O bond strength. On the other hand, the initiation rate was found to correlate strongly with the computed Ru–O bond strength. This latter finding enables both the rationalization and prediction of catalyst initiation through the calculation of a single thermodynamic parameter in which no assumptions about the mechanism of the initiation step are made.

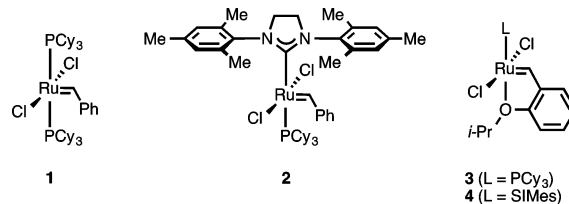


1. INTRODUCTION

Olefin metathesis is a powerful method for the synthesis of substituted alkenes.¹ Among the late transition metals that catalyze olefin metathesis, ruthenium has proven to be particularly useful in practical applications because of its tolerance for air, moisture, and heteroatom-containing functional groups.

During the past three decades, the field of ruthenium-catalyzed olefin metathesis has advanced rapidly, largely driven by the discovery and development of new catalysts with improved reactivity and selectivity (Chart 1).¹ In the early 1990s, our group developed a series of well-defined ruthenium-based olefin metathesis catalysts containing a stable ruthenium-alkylidene.² Since that time, the influence of various neutral (L-type) and anionic (X-type) ligands and alkylidene/benzylidene moieties has been extensively studied, leading to catalysts that are efficient in a range of transformations (e.g., 1 and 2).^{3,4} In 1999, Hoveyda and co-workers made an important discovery that the presence of an *o*-isopropoxybenzylidene led to chelated catalyst 3 in which the alkoxy group is coordinated at the axial site typically occupied by a phosphine ligand.⁵ Shortly thereafter, the Hoveyda^{6a} and Blechert^{6b} groups

Chart 1. Commonly Used Ruthenium-Based Olefin Metathesis Catalysts (1–4)^a



^aCy = cyclohexyl; SIMes = 1,3-bis(mesityl)-2-imidazolidinylidene.

extended this approach to the 1,3-bis(mesityl)-2-imidazolidinylidene (SIMes)-containing second-generation catalyst 4. The chelating benzylidene was found to impart exceptional stability to this family of catalysts, especially with respect to air and moisture. Moreover, the absence of phosphine ligands in 4 prevents certain phosphine-mediated catalyst decomposition

Received: February 5, 2015

Published: April 21, 2015

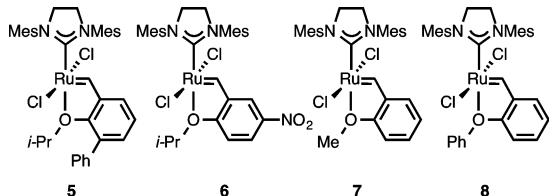
pathways.^{1g} Together, these properties have made **3**, **4**, and related catalysts useful tools in organic synthesis.¹

The rate of catalyst initiation is central to metathesis reactivity,^{7,8} and different initiation rates are optimal for different applications.^{1,9,10} Hence, the ability to rationally select a catalyst to achieve a desired initiation rate is practically important. However, with many systems, including Hoveyda-type catalysts, the initiation rate trends are not well understood, which hampers strategic selection of catalysts by end users.

Hoveyda-type catalysts initiate through an olefin metathesis reaction between the chelated ruthenium benzylidene and an olefin substrate. This reaction liberates one equivalent of an *o*-alkoxystyrene derivative and one equivalent of the propagating ruthenium alkylidene.⁸ Catalysts containing the classical chelating *o*-isopropoxybenzylidene are known to initiate slowly, which can be disadvantageous in some settings.^{1,9,10}

A large number of catalysts containing alternative chelating alkylidenes/benzylidenes have previously been reported,^{9–24} and it has been found empirically that catalyst initiation rates vary widely across this series. Several modifications have led to faster-initiating catalysts (e.g., **5–7**; Chart 2).^{12,14,20} Wakamatsu

Chart 2. Representative Known Fast-Initiating Catalysts with Hoveyda-Type Chelating Benzylidenes (5–8)



and Blechert discovered that the presence of an aryl group ortho to the isopropoxy group led to improved initiation (**5**), presumably through a buttressing effect in which the isopropyl group is pushed toward the equatorial chloride ligands, inducing unfavorable steric interactions.¹² Grela and co-workers found that an electron-withdrawing nitro group on the benzylidene also led to faster initiation (**6**).¹⁴ It is believed that the electron-withdrawing nature of the nitro group weakens the Ru=C and Ru–O bonds and renders the

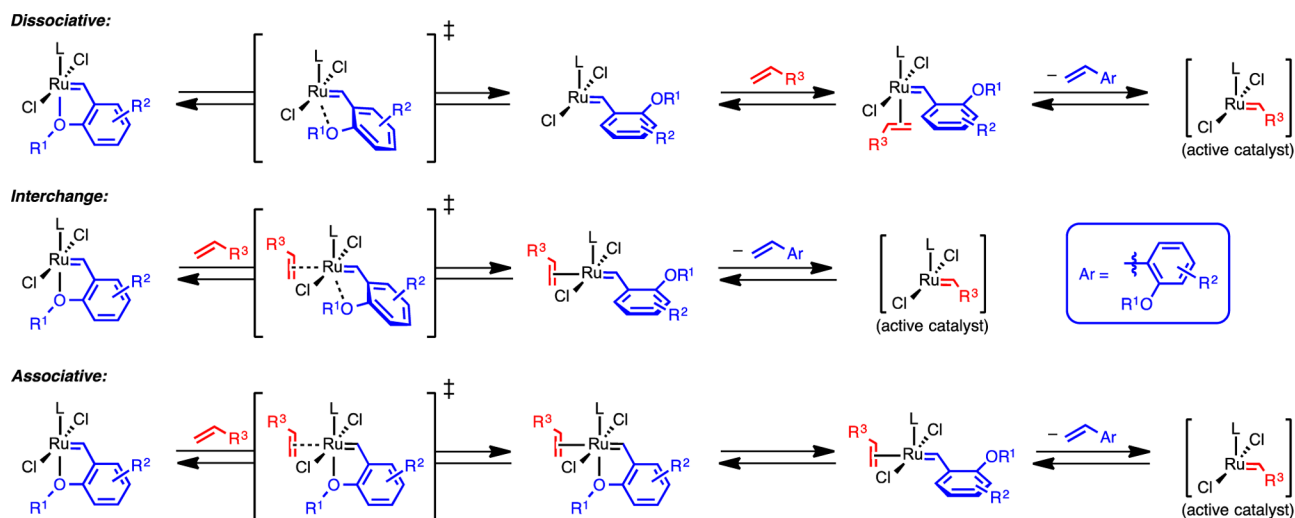
ruthenium center more electrophilic. Methoxy-substituted catalyst **7** was found by our group^{23b} and by Plenio¹⁹ to be faster-initiating than its isopropoxy congener, presumably as a result of attenuated steric hindrance around the ruthenium center and a less Lewis basic oxygen. Similarly, Plenio and co-workers recently found that catalyst **8** containing a phenoxy group is exceptionally fast-initiating.²⁰

There are several challenges in rationalizing and predicting initiation rates across this series. First, many of these catalysts have not been compared in standardized head-to-head assays to quantify initiation. Second, because the benzylidene structural modifications vary so widely among **4–8**, there are no obvious unifying physical organic parameters that would explain and predict initiation across this series. Third, the mechanism of initiation of Hoveyda-type catalysts is complex and is the topic of ongoing investigation in the literature (Scheme 1).²⁵ A recent mechanistic study by Plenio¹⁹ suggested that Hoveyda-type catalysts initiate by competing dissociative and interchange mechanisms, with the relative activation energies being a function of catalyst structure, olefin identity, and reaction conditions. In the absence of a clear mechanistic model, elucidating structure–activity relationships is difficult. The goal of the present investigation was to overcome these issues and develop a conceptual framework for rationalizing initiation rates of ruthenium olefin metathesis catalysts with chelated benzylidenes. In particular, we aimed to identify a parameter that would be effective for this purpose and could be determined *in silico* without making assumptions about the mechanism of catalyst initiation.

2. RESULTS

This problem was approached using a combination of organometallic synthesis, reaction kinetics, NMR spectroscopy, X-ray crystallography, and density functional theory (DFT) calculations. A structurally diverse collection of known and new catalysts were included in this study with the aim of obtaining insights that are generally applicable across the entire series of ruthenium olefin metathesis catalysts with chelating *o*-alkoxybenzylidenes. In particular, catalysts with sterically and electronically modified chelating benzylidene aryl groups (**5** and **6**) and alkoxy groups (**7–12**) were investigated. The

Scheme 1. Possible Initiation Mechanisms of Hoveyda-Type Catalysts, Including Transition State Structures for Proposed Rate-Limiting Steps

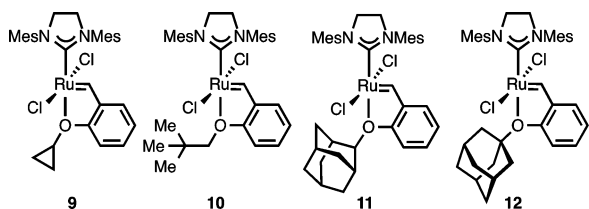


initiation rates across this series were found to vary over 2 orders of magnitude, representing a relatively wide range of reactivity profiles. X-ray crystal structures for all of the catalysts in this investigation were previously reported or were solved during the course of this study.

2.1. Synthesis and Reactivity of Catalysts with Modified Chelating Alkoxy Groups. Certain structural features of the chelating alkylidene/benzylidene moiety, especially the identity of the chelating functional group^{9,22} and the electronic properties of the benzylidene aryl ring,^{14–19} have been investigated in detail. Other structure–activity relationships, however, are less well understood. In particular, little is known about how variation of the chelating alkoxy group in Hoveyda-type catalysts (3 and 4) affects the initiation efficiency.^{23,24} The precedent of Blechert's catalyst 5^{12,13} and other reports^{23,24} suggested that variation of the steric and electronic properties of the alkoxy group would be an effective means of modulating initiation rate. Thus, to bridge this gap in knowledge, the first step in this investigation was to synthesize alkoxy-modified catalysts.

As an isopropyl group is of intermediate size, catalysts at the extremes of the steric spectrum were targeted (Chart 3). Thus,

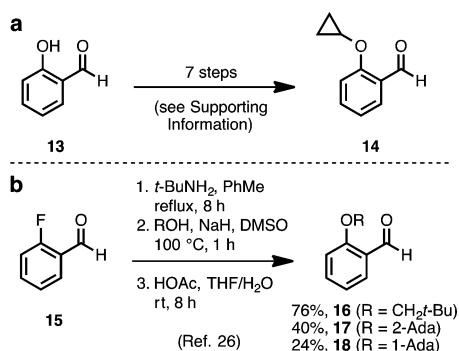
Chart 3. New Hoveyda-Type Catalysts Containing Alkoxy-Modified Chelating Benzylidenes (9–12)



to complement catalysts 7 and 8, which contain sterically small alkoxy/aryloxy groups that are weak Lewis bases, cyclopropyl catalyst 9 was prepared. At the other end of the spectrum, catalysts 10–12 with sterically bulky neopentyl, 2-adamantyl, and 1-adamantyl groups were also synthesized.

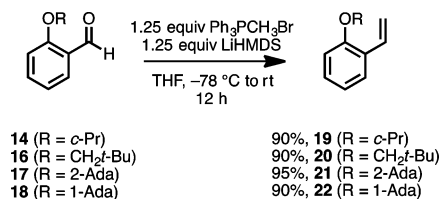
The investigation commenced with the synthesis of the desired catalysts according to the route shown in Schemes 2 and 3 and Table 1. To access catalysts of this type, a modular synthetic route using S_NAr chemistry was developed.²⁶ Cyclopropyl catalyst 9, however, could not be prepared in this way because of the instability of cyclopropoxide anion. Thus, a more circuitous sequence that relies on haloalkylation,

Scheme 2. Synthesis of Aldehyde Intermediates 14 and 16–18^a



^aFor detailed procedures, see the Supporting Information.

Scheme 3. Wittig Olefination To Prepare Styrenes 19–22^a



^aFor detailed procedures, see the Supporting Information.

Table 1. Complexation To Prepare 9–12^a

entry	styrene	R	product	yield (%)		
				method A	method B	method C
1	19	<i>c</i> -Pr	9	80	51	75
2	20	CH ₂ <i>t</i> -Bu	10	43	15	79
3	21	2-Ada	11	10–34	38	74
4	22	1-Ada	12	57–64	35	79

^aMethod A: 2 (0.2 mmol), styrene (0.2 mmol), and CuCl (0.2 mmol). Method B: 2 (0.2 mmol), styrene (0.4 mmol), and Amberlyst-15 (0.8 mmol). Method C: 23 (0.2 mmol), styrene (0.2 mmol), and Amberlyst-15 (0.8 mmol).

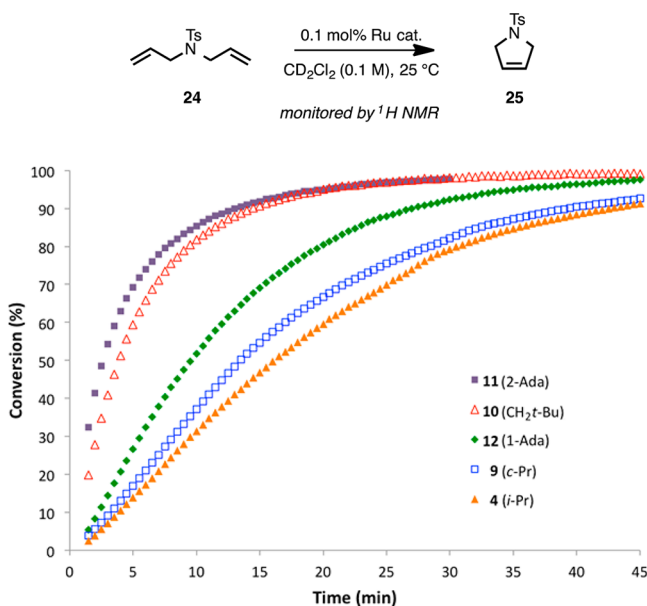
E2 elimination, Simmons–Smith cyclopropanation, and various protecting group manipulations was undertaken to prepare benzaldehyde 14 (Scheme 2a; also see the Supporting Information).²⁷ *o*-Alkoxybenzaldehydes 16–18 were prepared from 2-fluorobenzaldehyde in a more straightforward manner by the aforementioned S_NAr chemistry (Scheme 2b).²⁶ *o*-Alkoxybenzaldehydes 14 and 16–18 were then converted to styrenyl ethers 19–22 by Wittig olefination (Scheme 3).

Three methods were compared in the final complexation step (Table 1). In method A, second-generation SIMES/PCy₃-containing catalyst 2 was allowed to react with 1 equiv of 19–22 in the presence of CuCl as the phosphine scavenger. Precipitation to remove CuCl·PCy₃, filtration, and separation by silica gel column chromatography provided 9–12.^{6a} More strongly chelating benzylidenes, as in 9 (*c*-Pr) and 12 (1-Ada) (vide infra), were higher-yielding. Catalyst 11 (2-Ada) was problematic to prepare using method A and gave variable yields because of decomposition in solution outside of the glovebox. In method B, CuCl was replaced with Amberlyst-15 resin (immobilized H⁺)²⁸ and the loading of 19–22 was increased from 1 to 2 equiv. This procedure was operationally simpler, as purification consisted of filtration to remove the resin, sonication in pentane, filtration to collect the precipitated catalyst, and repeated washing with MeOH and pentane to remove impurities. The yields of 9–12 were generally lower than with method A, except in the case of 11 (2-Ada). Lastly, in method C, indenylidene monopyridine catalyst 23²⁹ was used in combination with 1 equiv of 19–22 and Amberlyst-15 resin.^{19,28} Following purification as in method B, catalysts 9–12 were obtained in high yield. Notably, the yields of 10 and 11 were markedly improved with method C compared with

methods A and B. This is likely due to the fact that the chelation strength in these catalysts is weak, which opens the possibility for secondary metathesis with the equivalent of alkene that is liberated from the progenitor catalyst (**2** or **23**). With **2** this alkene is styrene, while with **23** it is 1-methylene-3-phenyl-1*H*-indene. Because the latter is more substituted and thus more sterically hindered, secondary metathesis is slower. Overall, method C was optimal in terms of overall yield and operational convenience, particularly in the case of catalysts with weak chelation (**10** and **11**).^{30,31} Nevertheless, methods A and B could be useful in some contexts, given the widespread availability of starting catalyst **2**.

The catalytic reactivities of the four new catalysts were next determined by studying their performance in a representative ring-closing metathesis (RCM) reaction of *N*-tosyldiallylamine (**24**) using catalyst **4** as a benchmark (Scheme 4). The

Scheme 4. RCM Kinetics with Substrate **24 Using Various Catalysts, As Monitored by ¹H NMR Spectroscopy^a**



^aEach data point represents the average of three independent experiments.

reactions were carried out in triplicate with 0.1 mol % catalyst at 25 °C, and the reaction progress was monitored by ¹H NMR spectroscopy.^{32,33} With all five catalysts, RCM proceeded to >98% conversion within 90 min. Consistent with our hypothesis at the outset, the kinetic reactivity was found to be strongly dependent on the nature of the alkoxy group. The order of reactivity was found to be **11** (2-Ada) > **10** (CH₂*t*-Bu) > **12** (1-Ada) > **9** (*c*-Pr) > **4** (*i*-Pr). Catalytic metathesis reactions with the other catalysts in this study (**5–8**) have previously been demonstrated.^{12,14,20,23b}

2.2. Catalyst Initiation Rates. To quantify the catalyst initiation rates (k_{init}), the four new catalysts **9–12** were measured along with representative previously reported catalysts **4–8**. As discussed above, this particular set of catalysts was selected because it represents a wide variety of benzylidene modifications, including steric and electronic modification of the aryl ring and the alkoxy group. Initiation rates were determined by reacting a stoichiometric quantity of the catalyst with a large excess of butyl vinyl ether (BVE) (30 equiv) at 10

°C under pseudo-first-order conditions.⁷ The reaction progress was monitored by following the decay of the λ_{max} peak by UV/vis spectroscopy at regular intervals. The value of k_{init} for each catalyst was measured in triplicate, and the relative rate with respect to catalyst **4** (k_{rel}) was also calculated (Table 2).

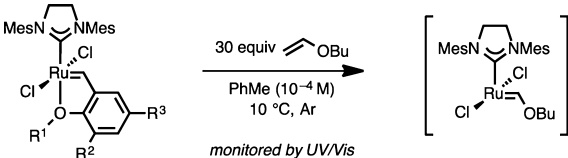
The initiation rates of **9–12** compared favorably with those of the known fast-initiating catalysts **5–8**. The order of the measured k_{init} values was consistent with the catalytic ¹H NMR data (Scheme 4). Among the catalysts tested, Blechert's catalyst **5** was found to be the fastest-initiating. Overall, these data demonstrate that the steric and electronic properties of the benzylidene play a major role in determining the initiation efficiency. Moreover, alkoxy group modification alone is capable of tuning the initiation rate over 2 orders of magnitude. The fact that isomeric catalysts **11** and **12** in particular display such different initiation rates, despite the fact that they both have a sterically bulky alkoxy substituent and differ only by the substitution position at the adamantyl group, was unexpected and merited further investigation (see section 3.2).

2.3. X-ray Crystal Structures and DFT-Optimized Structures. Structural, spectroscopic, and computational studies were next undertaken to understand the origins of the initiation rate trends in this series of catalysts and to test whether key metrics from these techniques correlated with the empirical initiation rates.

To this end, single crystals of Blechert's catalyst **5**¹² (the structure of which had not been previously reported; Chart 4) and the new catalysts **9–12** (Charts 5–8) suitable for X-ray diffraction were grown and analyzed.³⁴ These data confirmed the expected connectivity of the five catalysts. Catalysts **5** and **10** both crystallized in the *P2*₁/*c* space group. Catalyst **9** crystallized in the *Pna*2₁ space group with two crystallographically inequivalent conformers in the unit cell. Catalysts **11** and **12** were found to be isostructural, both crystallizing in the *Pca*2₁ space group with two inequivalent conformers in the unit cell. X-ray structures for **4** and **6–8** have been previously reported.^{20,23a,35}

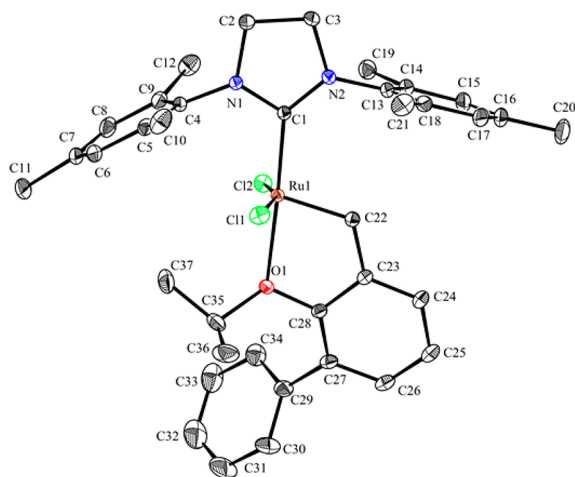
To complement the X-ray structures, the optimized geometries of **4–12** were located using several DFT methods that have been commonly employed in recent computational studies of ruthenium olefin metathesis catalysts.³⁶ We first considered two classical density functionals: B3LYP³⁷ with a mixed basis set of LANL2DZ for ruthenium and 6-31G(d) for other atoms—the level of theory that we have consistently used for geometry optimization in transition-metal-catalyzed reactions, including olefin metathesis with ruthenium catalysts—and BP86³⁸ with the SVP basis set, as recommended by Cavallo in a recent benchmark study on ruthenium complexes in olefin metathesis.³⁹ In addition, we tested three modern density functionals: M06,⁴⁰ M06-L,⁴¹ and ω B97x-D,⁴² which have been shown to give smaller errors for Ru–O and Ru–C bond lengths in previous benchmark studies by Truhlar and Jensen.⁴³ In the M06, M06-L, and ω B97x-D calculations, the SDD basis set for Ru and the 6-31G(d) basis set for other atoms were used.⁴⁴ The computed Ru–O and Ru=C(benzylidene) bond lengths are compiled and compared with the bond distances in the X-ray structures in Table 3.

In general, the Ru–O and Ru=C bond lengths remain fairly constant across this series. One striking exception is the long Ru–O bond in **11**, which is evident in both the experimental structures and optimized geometries at different theoretical levels. Elongation of the Ru–O bond occurs to relieve an energetically unfavorable steric clash between a methylene unit

Table 2. Initiation Rates of Catalysts 4–12, Displayed in Increasing Order^{a,b}


entry	cat.	R ¹	R ²	R ³	λ_{\max} (nm)	k_{init} (10^{-4} s ⁻¹)	k_{rel}
1	4	<i>i</i> -Pr	H	H	378	0.401 ± 0.037	1.0
2	9	<i>c</i> -Pr	H	H	376	0.721 ± 0.004	1.8
3	6	<i>i</i> -Pr	H	NO ₂	372	0.757 ± 0.054	1.9
4	7	Me	H	H	376	1.53 ± 0.09	3.8
5	12	1-Ada	H	H	382	3.46 ± 0.61	8.6
6	10	CH ₂ <i>f</i> -Bu	H	H	380	10.8 ± 0.8	26
7	8	Ph	H	H	370	49.1 ± 5.5	120
8	11	2-Ada	H	H	380	54.4 ± 5.6	140
9	5	<i>i</i> -Pr	Ph	H	374	98.5 ± 32.0	250

^aThe k_{init} values are reported as averages (with 95% confidence intervals) determined from three independent trials. ^bThe relative rate (k_{rel}) was calculated by dividing the k_{init} value of the catalyst of interest by the k_{init} value for catalyst 4.

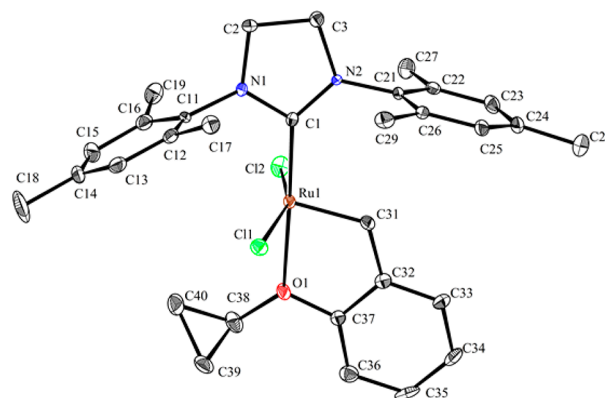
Chart 4. X-ray Crystal Structure of 5^a

^a50% probability ellipsoids. Hydrogen atoms have been omitted for clarity. Selected bond lengths (Å) for 5: Ru1–Cl1 2.34983(15), Ru1–Cl2 2.34349(15), Ru1–O1 2.2443(4), Ru1–C1 1.9808(5), Ru1–C22 1.8337(5). CCDC 1017843.³⁴

on the 2-Ada group (C35) and the SIMes–dichlororuthenium fragment.⁴⁵ The Ru–O bonds of catalysts 5, 9, 10, and 12 are of typical length, and no such obvious steric clash is observed. This unfavorable steric interaction contributes to 11's faster initiation compared with 12 (see section 3.2 for more detailed discussion).

Of the five computational methods, B3LYP and BP86 systematically overestimated the Ru–O bond lengths by about 0.1 Å, in line with the previous computational benchmark studies.⁴³ M06, M06-L, and ω B97x-D also led to longer Ru–O distances than the X-ray structures, while the mean absolute errors (MAEs) are smaller. However, since the Ru–O distances are very similar in most of the catalysts (except 11), all five methods tested yielded only moderate correlations between the computed and X-ray distances (see Charts S22–S26 in the Supporting Information).

Another point of interest in this collection of X-ray and DFT structures is that the *N*-Mes aryl rings on the alkoxy side are substantially puckered in many of the fast-initiating catalysts

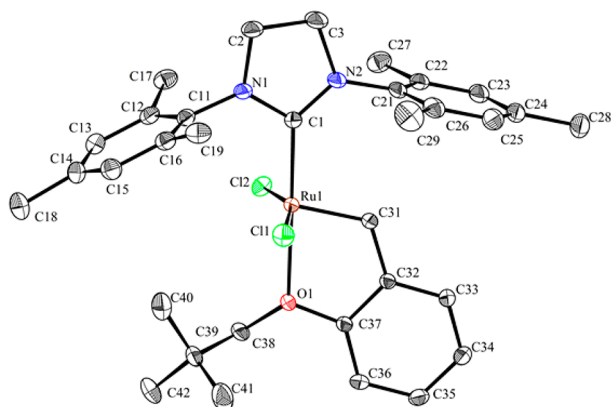
Chart 5. X-ray Crystal Structure of 9^a

^a50% probability ellipsoids. Hydrogen atoms have been omitted for clarity. Two crystallographically inequivalent molecules (A and B) are present in the unit cell; for clarity, only one is shown. Selected bond lengths (Å) for 9: molecule A: Ru1–Cl1 2.3377(14), Ru1–Cl2 2.3327(14), Ru1–O1 2.223(4), Ru1–C1 1.968(5), Ru1–C31 1.836(5); molecule B: Ru1–Cl1 2.3275(14), Ru1–Cl2 2.3312(13), Ru1–O1 2.249(4), Ru1–C1 1.985(5), Ru1–C31 1.830(5). CCDC 1044211.³⁴

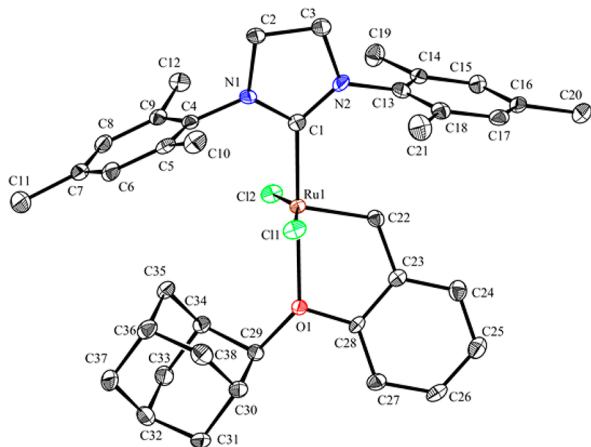
(5–12). These catalysts also show comparatively short *ipso*-C...Ru distances. These two observations are consistent with donation of the *p* orbital of the *ipso*-C to the metal center as a stabilizing interaction in cases where the Ru–O bond is comparatively weak.⁴⁶ For example, in the crystal structure of Hoveyda catalyst 4, the *ipso*-C...Ru distance is 3.307 Å,^{23a} compared with 3.151 Å in Blechert's catalyst 5.

2.4. NMR Spectroscopy. Diagnostic peaks from the ¹H and ¹³C NMR spectra in CD₂Cl₂ were next compiled (Table 4).^{12,14,47} The resulting data reveal a positive correlation between the initiation rate and the benzylidene ¹H NMR shift, a weak negative correlation between the initiation rate and the NHC ¹³C NMR shift, and no correlation between the benzylidene ¹³C NMR shift and the initiation rate. The relationship between initiation rates, Ru–O bond strengths, and NMR shifts is further discussed in section 3.3.

2.5. Computed Ru–O Bond Energies. To understand the relationship between the structural data and the observed

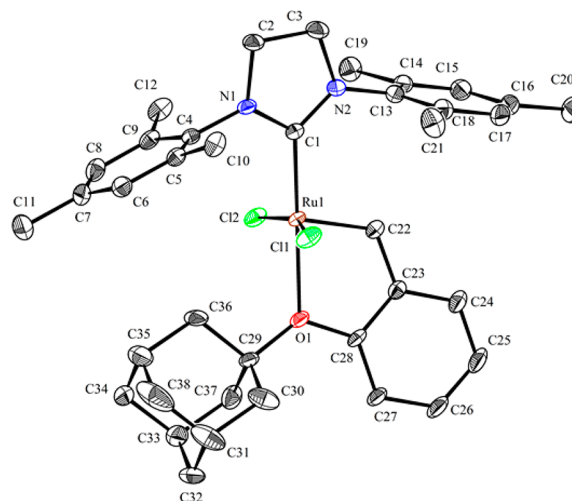
Chart 6. X-ray Crystal Structure of 10^a

^a50% probability ellipsoids. Hydrogen atoms and DCM solvent have been omitted for clarity. Selected bond lengths (Å) for **10**: Ru1–C11 2.3314(3), Ru1–C12 2.3270(3), Ru1–O1 2.2860(8), Ru1–C1 1.9848(10), Ru1–C31 1.8275(10). CCDC 1044212.³⁴

Chart 7. X-ray Crystal Structure of 11^a

^a50% probability ellipsoids. Hydrogen atoms have been omitted for clarity. Two crystallographically inequivalent molecules (A and B) are present in the unit cell; for clarity, only one is shown. Selected bond lengths (Å) for **11**: molecule A: Ru1–C11 2.3242(12), Ru1–C12 2.3570(11), Ru1–O1 2.338(3), Ru1–C1 1.984(4), Ru1–C22 1.827(4); molecule B: Ru1–C11 2.3220(11), Ru1–C12 2.3550(11), Ru1–O1 2.355(3), Ru1–C1 1.986(4), Ru1–C22 1.821(4). CCDC 1017842.³⁴

kinetic reactivity, the strengths of Ru–O bonding⁴⁸ in catalysts **4–12** were evaluated in two ways (Table 5): (1) by calculating the energy difference between the ground-state chelated conformation **A** and the nonchelated 14-electron complex **B** formed by dechelation of the Ru–O bond and rotation of the *o*-alkoxyphenyl group ($\Delta G_r(\mathbf{A} \rightarrow \mathbf{B})$) and (2) by calculating the reaction energy of initiation with BVE to form a common 14-electron Fischer carbene complex **C** ($\Delta G_r(\mathbf{A} \rightarrow \mathbf{C})$). These energies were calculated using M06 single-point calculations with a mixed basis set of SDD for ruthenium and 6-311+G(d,p) for other atoms and the SMD solvation model in toluene. The geometries were optimized with B3LYP/LANL2DZ–6-31G(d). Although B3LYP gave relatively large errors in the Ru–O distances, we found that employing B3LYP or BP86 in geometry optimization yielded better correlation between the computed Ru–O bond strengths and $\ln(k_{\text{init}})$ than the

Chart 8. X-ray Crystal Structure of 12^a

^a50% probability ellipsoids. Hydrogen atoms have been omitted for clarity. Two crystallographically inequivalent molecules (A and B) are present in the unit cell; for clarity, only one is shown. Selected bond lengths (Å) for **12**: molecule A: Ru1–C11 2.3190(6), Ru1–C12 2.3633(5), Ru1–O1 2.2540(14), Ru1–C1 1.9890(19), Ru1–C22 1.828(2); molecule B: Ru1–C11 2.3197(6), Ru1–C12 2.3645(6), Ru1–O1 2.2602(16), Ru1–C1 1.985(2), Ru1–C22 1.828(2). CCDC 1017841.³⁴

calculations using geometries optimized with M06, M06-L, or ω B97x-D (see the Supporting Information for details). In the following sections, all of the calculations were performed using B3LYP/LANL2DZ–6-31G(d) for geometry optimization and M06/SDD–6-311+G(d,p)/SMD(toluene) for single-point energies, which is consistent with our previous computational studies of ruthenium-catalyzed olefin metathesis.

The Ru–O bond strengths computed by the two methods correlated well with one another (Chart 9). The calculations indicated that the fast-initiating catalysts **8** (Ph), **11** (2-Ada), and Blechert's catalyst **5** all have a weaker Ru–O bond than catalysts **4**, **6**, and **9**.

3. DISCUSSION

The data from the approaches and techniques above were analyzed in detail to investigate the origins of the initiation rate trends and to correlate various metrics across this series.

3.1. Distortion Energies and Strain Release in the Initiation Step. An initial question concerned the relative importance of different factors to the Ru–O bond strengths in catalysts **4–12**. Two plausible contributions are (1) electronic effects that alter the charges on Ru and/or O and (2) the release of strain energy in the chelated catalyst. Thus, to test whether catalysts with weak Ru–O bonds and high initiation rates have high strain energies, we calculated the strain energies in the catalysts using distortion energy analysis.⁴⁹

The total strain energy of the chelated catalyst is dissected into the distortion energies of the SIMES–dichlororuthenium methylidene fragment and the alkoxyphenyl fragment. The distortion energy of each fragment is calculated from the energy difference between the geometry of the fragment in the chelated catalyst and the fully optimized geometry in the absence of the other fragment (see the Supporting Information for overlays of the distorted and fully optimized fragments).

Table 3. Summary of Experimental and Computed Ru–O and Ru=C Bond Distances for Representative Catalysts, Displayed in Order of Increasing k_{init}

entry	cat.	R ¹	R ²	R ³	bond distances (Å)											
					exptl		computed									
					X-ray ^a		B3LYP		BP86		M06		M06-L		ω B97x-D	
Ru–O	Ru=C	Ru–O	Ru=C	Ru–O	Ru=C	Ru–O	Ru=C	Ru–O	Ru=C	Ru–O	Ru=C					
1 ^b	4	<i>i</i> -Pr	H	H	2.256	1.829	2.36	1.85	2.35	1.85	2.31	1.82	2.33	1.84	2.29	1.82
2 ^c	9	<i>c</i> -Pr	H	H	2.236	1.833	2.34	1.85	2.33	1.85	2.28	1.83	2.31	1.85	2.26	1.82
3 ^{c,d}	6	<i>i</i> -Pr	H	NO ₂	2.273	1.827	2.39	1.84	2.37	1.85	2.33	1.82	2.34	1.84	2.31	1.81
4 ^e	7	Me	H	H	2.265	1.798	2.33	1.85	2.33	1.85	2.31	1.83	2.34	1.84	2.29	1.82
5 ^c	12	1-Ada	H	H	2.257	1.828	2.39	1.84	2.36	1.85	2.32	1.82	2.33	1.84	2.30	1.81
6 ^f	10	CH ₂ <i>t</i> -Bu	H	H	2.286	1.828	2.39	1.84	2.36	1.85	2.33	1.82	2.37	1.84	2.31	1.81
7 ^{c,g}	8	Ph	H	H	2.286	1.815	2.35	1.85	2.34	1.85	2.30	1.83	2.34	1.84	2.28	1.82
8 ^c	11	2-Ada	H	H	2.347	1.824	2.48	1.84	2.44	1.85	2.42	1.82	2.44	1.84	2.38	1.81
9	5	<i>i</i> -Pr	Ph	H	2.244	1.834	2.39	1.84	2.37	1.85	2.34	1.82	2.36	1.84	2.30	1.81
MAE: ^h					0.108	0.019	0.089	0.026	0.054	0.011	0.079	0.017	0.031	0.016		

^aFor clarity, experimental values are shown to three decimal places without estimated standard deviations. The estimated standard errors are typically in the range of 0.001–0.005 Å. See the Supporting Information for additional details. ^bExperimental: DCM solvate; CCDC 620588 (ref 23a). ^cThe experimental values are averages for the two crystallographically inequivalent molecules found in the unit cell. ^dExperimental: H₂O solvate; CCDC 698596 (ref 35). ^eExperimental: hexane solvate; CCDC 620589 (ref 23a). ^fExperimental: DCM solvate. ^gExperimental: CCDC 908389 (ref 20). ^hThe mean absolute error (MAE) is the average absolute error among the nine computed structures with respect to the crystallographic value.

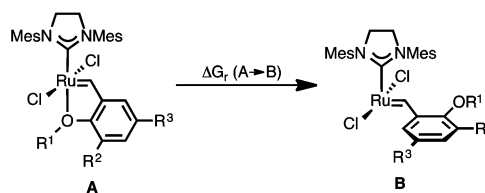
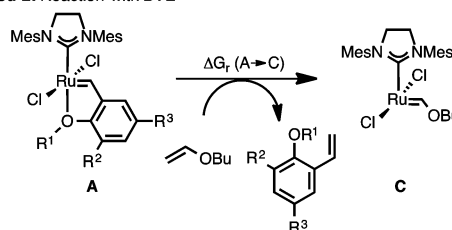
Table 4. Diagnostic NMR Peaks of Catalysts 4–12, Displayed in Order of Increasing k_{init}

entry	cat.	R ¹	R ²	R ³	Ru=CHAr		NHC
					¹ H	¹³ C	¹³ C
1 ^b	4	<i>i</i> -Pr	H	H	16.52	295.8	211.1
2	9	<i>c</i> -Pr	H	H	16.50	293.0	211.5
3 ^b	6	<i>i</i> -Pr	H	NO ₂	16.42	290.4 ^c	208.4
4	7	Me	H	H	16.48 ^c	290.4 ^c	210.5
5	12	1-Ada	H	H	16.48	300.0 ^c	211.7
6	10	CH ₂ <i>t</i> -Bu	H	H	16.58	295.9	210.4
7	8	Ph	H	H	16.64 ^c	290.7 ^c	209.3
8	11	2-Ada	H	H	16.69	298.9 ^c	209.2
9 ^b	5	<i>i</i> -Pr	Ph	H	16.62	298.2	210.6

^aSpectra in CD₂Cl₂. ^bThese values were independently measured and corresponded closely with previously published values in the literature: entry 1, ref 47; entry 3, ref 14; entry 9, ref 12. ^cAverage of two or more peaks corresponding to the benzylidene NMR peak.

The computed distortion energies of catalysts 4–12 are summarized in Chart 10.

In general, the sum of the distortion energies of the two fragments parallels the initiation rate. In particular, fast-initiating catalysts 11 and 5 show substantial distortion in the chelated structures, indicating that strain release is a key factor that controls the rate of initiation with these catalysts. The distortion in the alkoxybenzylidene moiety in Blechert's catalyst 5 is noticeably greater than that in the other catalysts. This indicates that the main driving force for this fast-initiating catalyst is the release of strain between the R¹ (*i*-Pr) and R² (Ph) groups in the catalyst, where Ru–O chelation forces the R¹ group to point toward R². Because of the steric repulsion between the 2-adamantyloxy group and the chloride ligands and/or *N*-Mes aryl group (see section 3.2 for more details), both the alkoxybenzylidene and SIMes–dichlororuthenium methylidene fragments in 11 are more distorted than those in 4. Similar, albeit weaker, steric repulsions with the alkoxy groups in 10 and 12 also lead to slightly greater distortion energies than in catalyst 4.

Table 5. Computed Ru–O Bond Strengths, Displayed in Order of Increasing k_{init} **Method 1: Dechelation****Method 2: Reaction with BVE**

entry	cat.	R ¹	R ²	R ³	Ru–O bond strength (kcal/mol)	
					$\Delta G_r(A \rightarrow B)$	$\Delta G_r(A \rightarrow C)$
1	4	<i>i</i> -Pr	H	H	12.8	6.3
2	9	<i>c</i> -Pr	H	H	10.8	4.6
3	6	<i>i</i> -Pr	H	NO ₂	14.1	5.8
4	7	Me	H	H	8.6	3.6
5	12	1-Ada	H	H	11.5	4.6
6	10	CH ₂ <i>t</i> -Bu	H	H	10.8	3.0
7	8	Ph	H	H	9.8	3.0
8	11	2-Ada	H	H	9.6	3.2
9	5	<i>i</i> -Pr	Ph	H	7.6	2.0

With certain catalysts, the distortion energies were lower than those for others in the series with similar initiation rates, including 6 (R¹ = *i*-Pr; R³ = NO₂), 7 (R¹ = Me), and 8 (R¹ = Ph). For example, 8 has a similar initiation rate and Ru–O bond strength to 11 but has 1.2 kcal/mol lower distortion energy. This indicates that strain release effects do not promote initiation in these complexes. Thus, this analysis revealed that strain release is the major factor for the observed enhanced

Chart 9. Ru–O Bond Strengths $\Delta G_r(A \rightarrow B)$ (Method 1) versus $\Delta G_r(A \rightarrow C)$ (Method 2)

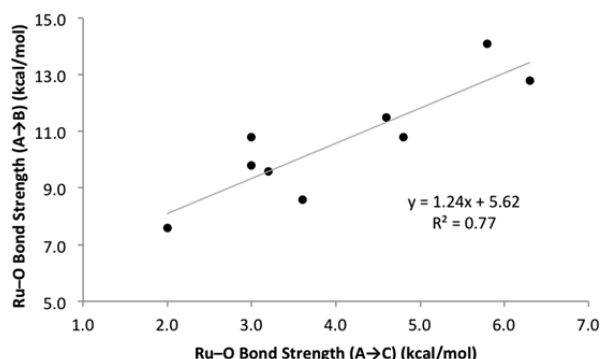
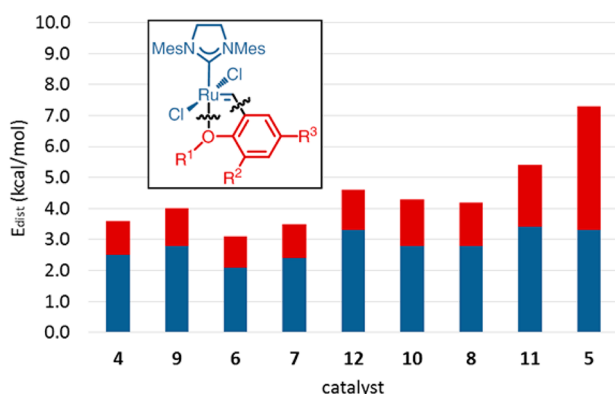


Chart 10. Computed Distortion Energies of the SIMes–Dichlororuthenium Methylidene Fragment (Shown in Blue) and the Alkoxyphenyl Fragment (Shown in Red) in Catalysts 4–12, Displayed from Left to Right in Order of Increasing k_{init}^a

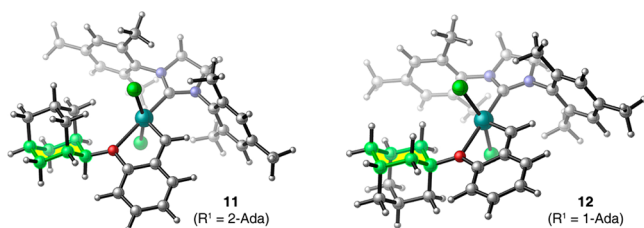


^aThe distortion energy of the fragment is defined as the difference between the energies of the distorted geometry of the fragment in the chelated catalyst and the fully optimized geometry in the absence of the other fragment.

initiation rates with 5, 11, 10, and 12, while the rates with catalysts 6, 7, and 8 are likely to be dominated by electronic effects.

3.2. Comparison of Catalysts 11 (2-Ada) and 12 (1-Ada). A structural basis for the observed reactivities of catalysts 11 and 12 is shown in Chart 11. As mentioned previously, an unfavorable methylene–*N*-Mes steric clash weakens the Ru–O bond in catalyst 11. This clash is ultimately the result of the unique geometry of the 2-Ada group and the conformationally restricted rotation about the alkoxy C–O bond. When the 2-Ada group is viewed as a substituted cyclohexane ring (green

Chart 11. Structural Basis for the Difference between the Initiation Rates of Catalysts 11 and 12

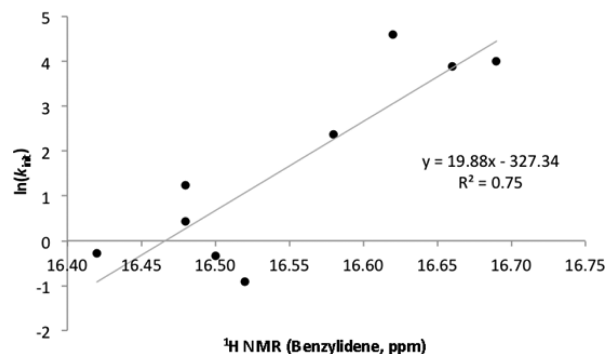


and yellow), it is evident that the majority of its steric bulk is directed toward the face of the *N*-Mes group and the chloride ligands. In contrast, the 1-Ada group orients its steric bulk away from the face of the *N*-Mes group and the chloride ligands. Rotation about the alkoxy C–O bond in 11 and 12 is restricted by developing $A^{1,3}$ strain with the ortho C–H bond. Additionally, the fact that the chelating alkoxy group in 11 contains a secondary carbon rather than a tertiary carbon as in 12 is also likely a contributing factor, since the former would be expected to be a weaker Lewis base.

3.3. Analysis of Collective Data. The metrics generated above were tested for possible correlation against the initiation rate in order to identify parameters that would be useful in both explanatory and predictive senses. First, structural metrics were compared with the $\ln(k_{\text{init}})$ values and Ru–O bond strengths. Generally in coordination chemistry, ligand–metal bond distances correlate with bond strengths. It was thus surprising that there was no correlation between the computed or experimental Ru–O bond lengths and the Ru–O bond strengths or $\ln(k_{\text{init}})$ values in this series (see Charts S28–S30 in the Supporting Information). More specifically, within the “normal” range for a Ru–O bond (approximately 2.24–2.29 Å), there is no relationship between the Ru–O bond strength and the Ru–O bond length. The only case in which an unusually long Ru–O bond was observed was in the 2-Ada catalyst 11, and it may be generally true that elongation of this bond can only be achieved in systems in which the alkoxy group is sterically hindered and conformationally constrained. Thus, the observation of a long Ru–O bond (>2.30 Å) in a SIMes-based Hoveyda-type catalyst likely indicates a weak Ru–O bond. However, the converse is not necessarily true; weak Ru–O bonds can and often do have “normal” Ru–O bond lengths (2.23–2.29 Å), as exemplified by catalyst 5. The lack of correlation in this respect is attributed to the intramolecular tethering of the ether ligand and the overall rigidity of the system. Because the structural data did not track with the initiation rates, other metrics were next considered.

As mentioned in section 2.4, NMR spectroscopy proved to be a useful tool in this respect. Ru–O bond strengths and $\ln(k_{\text{init}})$ values were found to correlate with the chemical shifts of key resonances in the ¹H and ¹³C NMR spectra (Table 4). In the case of the benzylidene ¹H NMR shift, there was a positive correlation with $\ln(k_{\text{init}})$ (Chart 12). This is consistent with a weaker Ru–O bond making the ruthenium center more electron-deficient, causing the C–H bond of the benzylidene to be deshielded. On the other hand, there was a weak negative correlation between $\ln(k_{\text{init}})$ and the NHC ¹³C NMR shift. This

Chart 12. $\ln(k_{\text{init}})$ versus Benzylidene ¹H NMR Shift



trend is consistent with a weaker Ru–O bond increasing the degree of π back-bonding from the metal to the NHC and exhibiting an attenuated trans influence. Grela's catalyst **6** was found to be an outlier, likely because of the strongly electron-withdrawing character of the NO₂ group. When **6** was excluded from the analysis, the R^2 value improved from 0.08 to 0.49. No correlation was found between $\ln(k_{\text{init}})$ and the benzyldiene ¹³C NMR shift (see Charts S31–S33 in the Supporting Information).

Of the quantitative measurements in this study, the computed Ru–O bond strengths in section 2.5 were the most informative (Charts 13 and 14). The initiation rate,

Chart 13. $\ln(k_{\text{init}})$ versus Ru–O Bond Strength $\Delta G_r(\text{A} \rightarrow \text{B})$ (Method 1)

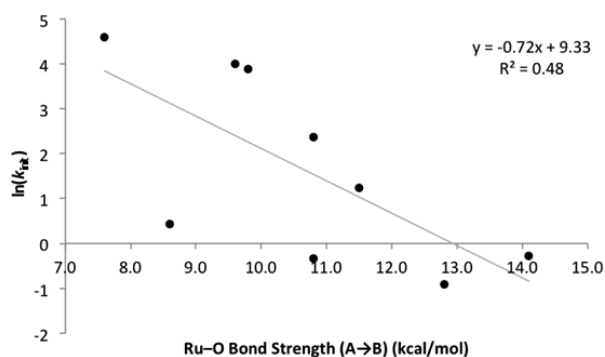
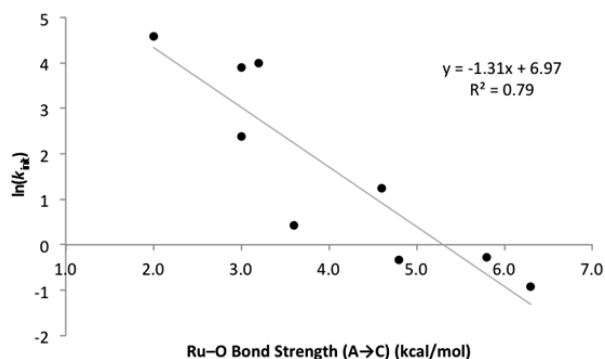


Chart 14. $\ln(k_{\text{init}})$ versus Ru–O Bond Strength $\Delta G_r(\text{A} \rightarrow \text{C})$ (Method 2)



$\ln(k_{\text{init}})$, correlated most strongly with $\Delta G_r(\text{A} \rightarrow \text{C})$ (method 2), while $\Delta G_r(\text{A} \rightarrow \text{B})$ (method 1) gave a weaker correlation. In both plots, the methyl-substituted catalyst **7** was found to be an outlier. Removal of this catalyst from the series improved the R^2 values from 0.48 to 0.73 and from 0.79 to 0.89 for methods 1 and 2, respectively (see Charts S34 and S35 in the Supporting Information). Using BP86 in place of B3LYP for the geometry optimizations improved the R^2 value with method 1 from 0.48 to 0.80 and led to similar R^2 values with method 2. Interestingly, using the M06, M06-L, and ω B97x-D methods in the geometry optimizations all led to worse R^2 values (see Tables S17–S20 in the Supporting Information).

While the exact mechanism of initiation of Hoveyda-type catalysts remains the topic of ongoing investigation in the literature,^{19,25,50} the correlation between the Ru–O bond energy and $\ln(k_{\text{init}})$ demonstrates that destabilizing the benzyldiene moiety by weakening the Ru–O bond leads to higher observed initiation rates. Herein we have delineated this

relationship quantitatively and constructed a model that echoes previous qualitative observations in the literature.^{12–25,35}

The Ru–O bond energies from the two methods presented above thus constitute powerful thermodynamic metrics for explaining and predicting the initiation kinetics in the absence of any assumptions about the mechanism of the initiation step. The fact that this thermodynamic metric is well-correlated to $\ln(k_{\text{init}})$ across a broad range of benzyldiene structures with different steric and electronic properties speaks to its generality and utility. Moreover, an attractive aspect of using *computed* Ru–O bond energies for this purpose is that predictions about a catalyst can be made without the need to first synthesize it.

An important caveat to this analysis is that there is almost certainly a lower limit beyond which weak Ru–O bonds no longer form stable chelates. Catalysts **5** and **11** appear to be close to this limit, as both show increased susceptibility to decomposition when dissolved in solution in air.

4. CONCLUSIONS

A systematic investigation was undertaken to understand factors that influence the initiation rates in a series of ruthenium olefin metathesis catalysts containing chelating benzyldienes. This study combined insights from organometallic synthesis, reaction kinetics, X-ray crystallography, NMR spectroscopy, and DFT calculations.

Four new second-generation catalysts, **9–12**, were synthesized, and all four exhibited improved initiation compared with the isopropoxy congener **4**. Catalyst **11** was found to be especially fast-initiating. The enhanced initiation rate is caused by a steric clash between a methylene group and the SIMes–dichlororuthenium fragment that is induced by the geometry of the 2-Ada group. This study demonstrates that alkoxy group modification alone is an effective strategy for tuning the initiation rate of Hoveyda-type catalysts over several orders of magnitude. It also illustrates the 2-Ada group as a unique alkyl substituent in coordination chemistry and catalysis.

Structural, spectroscopic, and computational insights on these new catalysts and several previously reported catalysts from the literature revealed the critical role of the Ru–O bond strength in the catalyst initiation rate. While the Ru–O bond strengths correlated with shifts of key resonances in the NMR spectra, no correlation was observed with the experimental or computed Ru–O bond distances. It is anticipated that this study will provide a conceptual framework for continuing efforts in catalyst development and will guide practitioners' selection of a specific catalyst for a given application. Moreover, in the long term, investigations of this nature will help enable prediction of new catalyst properties through computation.

■ ASSOCIATED CONTENT

Supporting Information

Experimental details, NMR spectra of new compounds, CIFs of catalysts **5** and **9–12**, optimized Cartesian coordinates and energies, and details of computational methods. This material is available free of charge via the Internet at <http://pubs.acs.org>.

■ AUTHOR INFORMATION

Corresponding Authors

*pengliu@pitt.edu
 *houk@chem.ucla.edu
 *rhg@caltech.edu

Notes

The authors declare no competing financial interest.

ACKNOWLEDGMENTS

Dr. Bruce S. Brunschwig is acknowledged for assistance with the UV/vis kinetics experiments, which were carried out at the Molecular Materials Research Center of the Beckman Institute at Caltech. Prof. Jeffrey S. Cannon (Occidental College) and Zachary K. Wickens (Grubbs group, Caltech) are thanked for helpful discussions. The research described herein was supported financially by the ONR (Award N00014-12-1-0596) and the NIH NIGMS (Award F32GM108145; postdoctoral fellowship to K.M.E.). The Bruker KAPPA APEXII X-ray diffractometer was purchased via an NSF CRIF:MU award to the California Institute of Technology (CHE-0639094). Materia, Inc. is thanked for the generous donation of catalysts **2**, **4**, **S16**, and **S17** and (*E/Z*)-1-isopropoxy-4-nitro-2-(prop-1-en-1-yl)benzene (**S20**). Calculations were performed on supercomputers from the DoD HPCMP Open Research Systems and the Extreme Science and Engineering Discovery Environment (XSEDE), which is supported by the NSF.

REFERENCES

- (1) For reviews, see: (a) Trnka, T. M.; Grubbs, R. H. *Acc. Chem. Res.* **2001**, *34*, 18–29. (b) Fürstner, A. *Angew. Chem., Int. Ed.* **2000**, *39*, 3012–3043. (c) Schrock, R. R.; Hoveyda, A. H. *Angew. Chem., Int. Ed.* **2003**, *42*, 4592–4633. (d) Nicolaou, K. C.; Bulger, P. G.; Sarlah, D. *Angew. Chem., Int. Ed.* **2005**, *44*, 4490–4527. (e) Schrock, R. R. *Chem. Rev.* **2009**, *109*, 3211–3226. (f) Samojłowicz, C.; Bieniek, M.; Grela, K. *Chem. Rev.* **2009**, *109*, 3708–3742. (g) Vougioukalakis, G. C.; Grubbs, R. H. *Chem. Rev.* **2010**, *110*, 1746–1787. (h) Hoveyda, A. H. *J. Org. Chem.* **2014**, *79*, 4763–4792. (i) Nelson, D. J.; Manzini, S.; Urbina-Blanco, C. A.; Nolan, S. P. *Chem. Commun.* **2014**, *50*, 10355–10375.
- (2) (a) Nguyen, S. T.; Johnson, L. K.; Grubbs, R. H.; Ziller, J. W. *J. Am. Chem. Soc.* **1992**, *114*, 3974–3975. (b) Nguyen, S. T.; Grubbs, R. H.; Ziller, J. W. *J. Am. Chem. Soc.* **1993**, *115*, 9858–9859.
- (3) (a) Schwab, P.; France, M. B.; Ziller, J. W.; Grubbs, R. H. *Angew. Chem., Int. Ed. Engl.* **1995**, *34*, 2039–2041. (b) Schwab, P.; Grubbs, R. H.; Ziller, J. W. *J. Am. Chem. Soc.* **1996**, *118*, 100–110.
- (4) Scholl, M.; Ding, S.; Lee, C. W.; Grubbs, R. H. *Org. Lett.* **1999**, *1*, 953–956.
- (5) (a) Kingsbury, J. S.; Harrity, J. P. A.; Bonitatebus, P. J., Jr.; Hoveyda, A. H. *J. Am. Chem. Soc.* **1999**, *121*, 791–799. For a review, see: (b) Hoveyda, A. H.; Gillingham, D. G.; Van Veldhuizen, J. J.; Kataoka, O.; Garber, S. B.; Kingsbury, J. S.; Harrity, J. P. A. *Org. Biomol. Chem.* **2004**, *2*, 8–23.
- (6) (a) Garber, S. B.; Kingsbury, J. S.; Gray, B. L.; Hoveyda, A. H. *J. Am. Chem. Soc.* **2000**, *122*, 8168–8179. (b) Gessler, S.; Randl, S.; Blechert, S. *Tetrahedron Lett.* **2000**, *41*, 9973–9976.
- (7) Sanford, M. S.; Love, J. A.; Grubbs, R. H. *J. Am. Chem. Soc.* **2001**, *123*, 6543–6554.
- (8) After initiation, the benzylidene moiety is no longer attached to the catalyst, meaning that the propagating species for catalysts **4–12** and other second-generation catalysts will be identical. For this reason, the initiation rate, the rate of *o*-alkoxystyrene rechelation, and the rates of various catalyst decomposition events are the most crucial variables to consider when comparing a series of catalysts in which the benzylidene moiety is varied.
- (9) For a review of ruthenium olefin metathesis catalysts containing chelating benzylidenes, see: Vidavsky, Y.; Anaby, A.; Lemcoff, N. G. *Dalton Trans.* **2012**, *41*, 32–43.
- (10) For an illustrative application of catalyst **6** in macrocyclic RCM on a process scale, see: (a) Shu, C.; Zeng, X.; Hao, M.-H.; Wei, X.; Yee, N. K.; Busacca, C. A.; Han, Z.; Farina, V.; Senanayake, C. H. *Org. Lett.* **2008**, *10*, 1303–1306. (b) Farina, V.; Shu, C.; Zeng, X.; Wei, X.; Han, Z.; Yee, N. K.; Senanayake, C. H. *Org. Process Res. Dev.* **2009**, *13*, 250–254.
- (11) Wakamatsu, H.; Blechert, S. *Angew. Chem., Int. Ed.* **2002**, *41*, 794–796.
- (12) Wakamatsu, H.; Blechert, S. *Angew. Chem., Int. Ed.* **2002**, *41*, 2403–2405.
- (13) The Blechert chelate (as in **5**) has been successfully used to improve initiation in ruthenium catalysts with a wide variety of L- and X-type ligands. For examples, see: (a) Van Veldhuizen, J. J.; Gillingham, D. G.; Garber, S. B.; Kataoka, O.; Hoveyda, A. H. *J. Am. Chem. Soc.* **2003**, *125*, 12502–12508. (b) Berlin, J. M.; Campbell, K.; Ritter, T.; Funk, T. W.; Chlenov, A.; Grubbs, R. H. *Org. Lett.* **2007**, *9*, 1339–1342. (c) Gatti, M.; Vieille-Petit, L.; Luan, X.; Mariz, R.; Drinkel, E.; Linden, A.; Dorta, R. *J. Am. Chem. Soc.* **2009**, *131*, 9498–9499.
- (14) Grela, K.; Harutyunyan, S.; Michrowska, A. *Angew. Chem., Int. Ed.* **2002**, *41*, 4038–4040.
- (15) Zaja, M.; Connon, S. J.; Dunne, A. M.; Rivard, M.; Buschmann, N.; Jiricek, J.; Blechert, S. *Tetrahedron* **2003**, *59*, 6545–6558.
- (16) Zhan, Z.-Y. J. Recyclable Ruthenium Catalysts for Metathesis Reactions. U.S. Patent US20070043180 A1, Feb 22, 2007.
- (17) Vinokurov, N.; Garabatos-Perera, J. R.; Zhao-Karger, Z.; Wiebecke, M.; Butenschön, H. *Organometallics* **2008**, *27*, 1878–1886.
- (18) Rix, D.; Caijo, F.; Laurent, I.; Boeda, F.; Clavier, H.; Nolan, S. P.; Mauduit, M. *J. Org. Chem.* **2008**, *73*, 4225–4228.
- (19) Thiel, V.; Hendann, M.; Wannowius, K.-J.; Plenio, H. *J. Am. Chem. Soc.* **2012**, *134*, 1104–1114.
- (20) Kos, P.; Savka, R.; Plenio, H. *Adv. Synth. Catal.* **2013**, *355*, 439–447.
- (21) Nelson, D. J.; Queval, P.; Rouen, M.; Magrez, M.; Toupet, L.; Caijo, F.; Borré, E.; Laurent, I.; Crévisy, C.; Baslé, O.; Mauduit, M.; Percy, J. M. *ACS Catal.* **2013**, *3*, 259–264.
- (22) For representative reports describing alternative chelating functional groups, see: (a) van der Schaaf, P. A.; Kolly, R.; Kirner, H.-J.; Rime, F.; Mühlbach, A.; Hafner, A. *J. Organomet. Chem.* **2000**, *606*, 65–74. (b) Fürstner, A.; Thiel, O. R.; Lehmann, C. W. *Organometallics* **2002**, *21*, 331–335. (c) Slugovc, C.; Perner, B.; Stelzer, F.; Mereiter, K. *Organometallics* **2004**, *23*, 3622–3626. (d) Barbasiewicz, M.; Szadkowska, A.; Bujok, R.; Grela, K. *Organometallics* **2006**, *25*, 3599–3604. (e) Hejl, A.; Day, M. W.; Grubbs, R. H. *Organometallics* **2006**, *25*, 6149–6154. (f) Ben-Asuly, A.; Tzur, E.; Diesendruck, C. E.; Sigalov, M.; Goldberg, I.; Lemcoff, N. G. *Organometallics* **2008**, *27*, 811–813. (g) Kost, T.; Sigalov, M.; Goldberg, I.; Ben-Asuly, A.; Lemcoff, N. G. *J. Organomet. Chem.* **2008**, *693*, 2200–2203. (h) Tzur, E.; Szadkowska, A.; Ben-Asuly, A.; Makal, A.; Goldberg, I.; Woźniak, K.; Grela, K.; Lemcoff, N. G. *Chem.—Eur. J.* **2010**, *16*, 8726–8737. (i) Szadkowska, A.; Żukowska, K.; Pazio, A. E.; Woźniak, K.; Kadyrov, R.; Grela, K. *Organometallics* **2011**, *30*, 1130–1138. (j) Ginzburg, Y.; Anaby, A.; Vidavsky, Y.; Diesendruck, C. E.; Ben-Asuly, A.; Goldberg, I.; Lemcoff, N. G. *Organometallics* **2011**, *30*, 3430–3437. (k) Lexer, C.; Burtscher, D.; Perner, B.; Tzur, E.; Lemcoff, N. G.; Slugovc, C. *J. Organomet. Chem.* **2011**, *696*, 2466–2470. (l) Peeck, L. H.; Savka, R. D.; Plenio, H. *Chem.—Eur. J.* **2012**, *18*, 12845–12853. (m) Barbasiewicz, M.; Michalak, M.; Grela, K. *Chem.—Eur. J.* **2012**, *18*, 14237–14241.
- (23) For relevant reports, see refs 5, 18, and 19 and the following: (a) Barbasiewicz, M.; Bieniek, M.; Michrowska, A.; Szadkowska, A.; Makal, A.; Woźniak, K.; Grela, K. *Adv. Synth. Catal.* **2007**, *349*, 193–203. (b) Hejl, A. Ph.D. Thesis, California Institute of Technology, Pasadena, CA, 2007. (c) Bornand, M.; Torker, S.; Chen, P. *Organometallics* **2007**, *26*, 3585–3596.
- (24) For multidentate chelating alkoxy-derived benzylidenes, see: (a) Bieniek, M.; Bujok, R.; Cabaj, M.; Lugan, N.; Lavigne, G.; Arlt, D.; Grela, K. *J. Am. Chem. Soc.* **2006**, *128*, 13652–13653. (b) Bieniek, M.; Samojłowicz, C.; Sashuk, V.; Bujok, R.; Śledź, P.; Lugan, N.; Lavigne, G.; Arlt, D.; Grela, K. *Organometallics* **2011**, *30*, 4144–4158.
- (25) For reports concerning the initiation mechanism of Hoveyda-type catalysts, see refs 19 and 23b and the following: (a) Vougiouka-

lakis, G. C.; Grubbs, R. H. *Chem.—Eur. J.* **2008**, *14*, 7545–7556. (b) Solans-Monfort, X.; Pleixats, R.; Sodupe, M. *Chem.—Eur. J.* **2010**, *16*, 7331–7343. (c) Vorfalt, T.; Wannowius, K.-J.; Plenio, H. *Angew. Chem., Int. Ed.* **2010**, *49*, 5533–5536. (d) Ashworth, I. W.; Hillier, I. H.; Nelson, D. J.; Percy, J. M.; Vincent, M. A. *Chem. Commun.* **2011**, *47*, 5428–5430. (e) Nuñez-Zarur, F.; Solans-Monfort, X.; Rodríguez-Santiago, L.; Sodupe, M. *Organometallics* **2012**, *31*, 4203–4215. (f) Ashworth, I. W.; Hillier, I. H.; Nelson, D. J.; Percy, J. M.; Vincent, M. A. *ACS Catal.* **2013**, *3*, 1929–1939.

(26) Engle, K. M.; Luo, S.-X.; Grubbs, R. H. *J. Org. Chem.* **2015**, *80*, 4213–4220.

(27) (a) Cote, B.; Ducharme, Y.; Frenette, R.; Friesen, R.; Martins, E. (Merck & Co.). Tri-aryl-substituted-ethane PDE4 Inhibitors. U.S. Patent US20020156105 A1, Oct 24, 2002. (b) Cherian, J.; Choi, I.; Nayyar, A.; Manjunatha, U. H.; Mukherjee, T.; Lee, Y. S.; Boshoff, H. I.; Singh, R.; Ha, Y. H.; Goodwin, M.; Lakshminarayana, S. B.; Niyomrattanakit, P.; Jiricek, J.; Ravindran, S.; Dick, T.; Keller, T. H.; Dartois, V.; Barry, C. E., III *J. Med. Chem.* **2011**, *54*, 5639–5659.

(28) Monsaert, S. F.; Verpoort F. W. C. (Umicore AG & Co. KG and Ghent University). Process for Preparation of Ruthenium-Based Carbene Catalysts with Chelating Alkylidene Ligands. World Patent WO2011091980 A1, Aug 4, 2011.

(29) (a) Monsaert, S.; Drozdak, R.; Dragutan, V.; Dragutan, I.; Verpoort, F. *Eur. J. Inorg. Chem.* **2008**, 432–440. (b) Urbina-Blanco, C. A.; Manzini, S.; Gomes, J. P.; Doppiu, A.; Nolan, S. P. *Chem. Commun.* **2011**, *47*, 5022–5024. For a relevant review, see: (c) Boeda, F.; Clavier, H.; Nolan, S. P. *Chem. Commun.* **2008**, 2726–2740.

(30) Catalysts **9–12** are air-stable, free-flowing green solids that can be conveniently stored and manipulated as solids outside of the glovebox. In solution, however, catalyst **11** is susceptible to decomposition when dissolved in organic solvents that have not been rigorously dried and degassed. It is recommended that standard Schlenk techniques be employed when **11** is used outside of the glovebox. Catalysts **9**, **10**, and **12** are more robust toward air and moisture in solution and can be handled in organic solvents that have not been rigorously dried or degassed. Across the series of catalysts that were examined in this study (**4–12**), it was found that faster-initiating catalysts tended to be more susceptible to decomposition in solvents that were not rigorously dried and degassed. It is likely that decomposition is mediated by trace quantities of dissolved O₂. For relevant discussion, see ref 21.

(31) The procedures using Amberlyst-15 resin are advantageous in terms of operational simplicity, as they do not require purification by silica gel column chromatography. Instead, the workup involves precipitation, filtration, and repeated washing with MeOH and pentane. With **11**, precipitating the catalyst immediately and purifying it through a series of washes is important because the catalyst decomposes when dissolved in organic solvents that have not been rigorously dried and degassed.

(32) RCM kinetics experiments were performed according to a previously published procedure. See: Ritter, T.; Hejl, A.; Wenzel, A. G.; Funk, T. W.; Grubbs, R. H. *Organometallics* **2006**, *25*, 5740–5745.

(33) For consistent results in RCM kinetics, the purity of the solvent and the diene were found to be critical. See the Supporting Information.

(34) CCDC 1017843 (**5**), 1044211 (**9**), 1044212 (**10**), 1017842 (**11**), and 1017841 (**12**) contain the supplementary crystallographic data for this paper. These data can be obtained free of charge from The Cambridge Crystallographic Data Centre via www.ccdc.cam.ac.uk/data_request/cif.

(35) Barbasiewicz, M.; Szadkowska, A.; Makal, A.; Jarzemska, K.; Woźniak, K.; Grela, K. *Chem.—Eur. J.* **2008**, *14*, 9330–9337.

(36) All of the computations were performed in the gas phase with Gaussian 09: Frisch, M. J.; Trucks, G. W.; Schlegel, H. B.; Scuseria, G. E.; Robb, M. A.; Cheeseman, J. R.; Scalmani, G.; Barone, V.; Mennucci, B.; Petersson, G. A.; Nakatsuji, H.; Caricato, M.; Li, X.; Hratchian, H. P.; Izmaylov, A. F.; Bloino, J.; Zheng, G.; Sonnenberg, J. L.; Hada, M.; Ehara, M.; Toyota, K.; Fukuda, R.; Hasegawa, J.; Ishida, M.; Nakajima, T.; Honda, Y.; Kitao, O.; Nakai, H.; Vreven, T.;

Montgomery, J. A., Jr.; Peralta, J. E.; Ogliaro, F.; Bearpark, M.; Heyd, J. J.; Brothers, E.; Kudin, K. N.; Staroverov, V. N.; Kobayashi, R.; Normand, J.; Raghavachari, K.; Rendell, A.; Burant, J. C.; Iyengar, S. S.; Tomasi, J.; Cossi, M.; Rega, N.; Millam, J. M.; Klene, M.; Knox, J. E.; Cross, J. B.; Bakken, V.; Adamo, C.; Jaramillo, J.; Gomperts, R.; Stratmann, R. E.; Yazyev, O.; Austin, A. J.; Cammi, R.; Pomelli, C.; Ochterski, J. W.; Martin, R. L.; Morokuma, K.; Zakrzewski, V. G.; Voth, G. A.; Salvador, P.; Dannenberg, J. J.; Dapprich, S.; Daniels, A. D.; Farkas, Ö.; Foresman, J. B.; Ortiz, J. V.; Cioslowski, J.; Fox, D. J. *Gaussian 09*, revision D.01; Gaussian, Inc.: Wallingford, CT, 2009.

(37) (a) Lee, C.; Yang, W.; Parr, R. G. *Phys. Rev. B* **1988**, *37*, 785–789. (b) Stephens, P. J.; Devlin, F. J.; Chabalowski, C. F.; Frisch, M. J. *J. Phys. Chem.* **1994**, *98*, 11623–11627.

(38) (a) Becke, A. D. *Phys. Rev. A* **1988**, *38*, 3098–3100. (b) Perdew, J. P. *Phys. Rev. B* **1986**, *33*, 8822–8824.

(39) (a) Poater, A.; Pump, E.; Vummaleti, S. V. C.; Cavallo, L. *J. Chem. Theory Comput.* **2014**, *10*, 4442–4448. For earlier examples using BP86 to study ruthenium-catalyzed olefin metathesis reactions, see: (b) Adlhart, C.; Chen, P. *Angew. Chem., Int. Ed.* **2002**, *41*, 4484–4487. (c) Diesendruck, C. E.; Tzur, E.; Ben-Asuly, A.; Goldberg, I.; Straub, B. F.; Lemcoff, N. G. *Inorg. Chem.* **2009**, *48*, 10819–10825.

(40) Zhao, Y.; Truhlar, D. G. *Theor. Chem. Acc.* **2008**, *120*, 215–241.

(41) Zhao, Y.; Truhlar, D. G. *J. Chem. Phys.* **2006**, *125*, 194101.

(42) Chai, J.-D.; Head-Gordon, M. *Phys. Chem. Chem. Phys.* **2008**, *10*, 6615–6620.

(43) (a) Kulkarni, A. D.; Truhlar, D. G. *J. Chem. Theory Comput.* **2011**, *7*, 2325–2332. (b) Minenkov, Y.; Singstad, Å.; Occhipinti, G.; Jensen, V. R. *Dalton Trans.* **2012**, *41*, 5526–5541.

(44) Here we used computationally less-demanding double- ζ basis sets in the geometry optimizations since the previous benchmark studies revealed relatively small differences between double- and triple- ζ basis sets in geometry optimizations of ruthenium complexes. See refs 39a and 43a.

(45) The 2-Ada group in catalyst **11** is oriented closer to one of the *N*-Mes aryl rings and to the chloride ligands than the *i*-Pr and 1-Ada groups in catalysts **4** and **12**, respectively. See the Supporting Information.

(46) (a) Stüßner, M.; Plenio, H. *Chem. Commun.* **2005**, 5417–5419. (b) Leuthäuser, S.; Schmidts, V.; Thiele, C. M.; Plenio, H. *Chem.—Eur. J.* **2008**, *14*, 5465–5481. (c) Credendino, R.; Falivene, L.; Cavallo, L. *J. Am. Chem. Soc.* **2012**, *134*, 8127–8135.

(47) (a) Vehlow, K.; Maechling, S.; Blechert, S. *Organometallics* **2006**, *25*, 25–28. (b) Vehlow, K.; Maechling, S.; Köhler, K.; Blechert, S. *J. Organomet. Chem.* **2006**, *691*, 5267–5277.

(48) These thermodynamic values are a means of measuring the strengths of Ru–O bonding interactions. Though they are not bond dissociation energies in a classical sense, throughout the text we refer to these values as “bond strengths” in the interest of brevity.

(49) For applications of distortion/interaction analysis in organometallic chemistry, see: (a) Gorelsky, S. I.; Lapointe, D.; Fagnou, K. *J. Am. Chem. Soc.* **2008**, *130*, 10848–10849. (b) Green, A. G.; Liu, P.; Merlic, C. A.; Houk, K. N. *J. Am. Chem. Soc.* **2014**, *136*, 4575–4583. For computational studies of strain energies using the fragmentation approach, see: (c) Fernández, I.; Bickelhaupt, F. M.; Cossío, F. P. *Chem.—Eur. J.* **2012**, *18*, 12395–12403. (d) Fernández, I.; Bickelhaupt, F. M.; Cossío, F. P. *Chem.—Eur. J.* **2014**, *20*, 10791–10801.

(50) One model is that Hoveyda-type catalysts initiate by competing dissociative and interchange mechanisms. For a detailed discussion, see ref 19 and references therein. In both mechanisms, a weaker Ru–O bond would decrease the activation barrier for initiation. For example, because of the weaker Ru–O bond, the computed barrier for the dissociative initiation pathway of **11** is 1.7 kcal/mol lower than that of **4**. See the Supporting Information for details.